PHYSICAL REVIEW D **86,** 094507 (2012)

Lattice QCD study of the $K^*(892)$ meson decay width

Ziwen Fu[1,*] and Kan Fu[2,†]

[1]*Key Laboratory of Radiation Physics and Technology (Sichuan University), Ministry of Education, Institute of Nuclear Science and Technology, College of Physical Science and Technology, Sichuan University, Chengdu 610064, People's Republic of China*
[2]*School of Environment, Tsinghua University, Peking 100084, People's Republic of China*

(Received 31 August 2012; published 7 November 2012)

We deliver an exploratory lattice QCD examination of the $K^*(892)$ meson decay width via the p-wave scattering phase shift of a pion-kaon (πK) system in the isospin $I = 1/2$ channel. The modified Rummukainen-Gottlieb formula for a two-particle system with arbitrary mass is employed to extract phase shifts, which clearly reveal the existence of a resonance at a mass around the $K^*(892)$ meson mass. The effective range formula is applied to describe the energy dependence of the phase shift and we extract the effective $K^* \to \pi K$ coupling constant as $g_{K^*\pi K} = 6.38(78)$. The decay width estimated from the phase shift is about 64.9 ± 8.0 MeV, which is in reasonable accordance with the experiment. Our lattice investigations are conducted on a $20^3 \times 48$ MILC gauge configuration with the $N_f = 2 + 1$ flavors of the asqtad-improved staggered dynamical sea quarks at $(m_\pi + m_K)/m_{K^*} \approx 0.739$ and lattice spacing $a \approx 0.15$ fm.

DOI: 10.1103/PhysRevD.86.094507 PACS numbers: 12.38.Gc, 11.15.Ha

I. INTRODUCTION

It is well-known that the $K^*(892)$ meson is a resonance. In 2012, the Particle Data Group (PDG) listed the $K^*(892)$ meson $I(J^P) = \frac{1}{2}(1^-)$, with a mass of 891.66 ± 0.26 MeV and a narrow width of 50.8 ± 0.9 MeV [1]. Some recent experimental analyses [2–6] have precisely measured its resonance parameters. Moreover, several theoretical efforts have been undertaken to calculate its hadronic coupling constants [7–9]. Since the $K^*(892)$ meson is a low-lying vector meson with strangeness, a study of its decay width is definitely a straightforward probing of the three-flavor structure of the low-energy hadronic interactions; thus, it is very helpful for us to comprehend the dynamical trait of the hadron reactions with QCD.

The most feasible approach to extract the resonance parameters of the vector $K^*(892)$ meson nonperturbatively from first principles is to resort to lattice QCD. The principal decay channel (with a branching rate of 99.9%) of the $K^*(892)$ meson is to one pion and one kaon in the p-wave [1], which can then be precisely dealt with on the lattice, and there is a pioneering quenched lattice QCD study on its coupling constant $g_{K^*\pi K}$ through evaluating the appropriate three-point correlation function [10]. Among unstable hadrons, the vector ρ meson is ideal (see reasons in Ref. [11]) for lattice QCD investigations of a resonance, and it is extensively studied [10–18]; nevertheless, so far, lattice QCD research on the resonance parameters of the $K^*(892)$ meson directly from the p-wave πK scattering phase in the $I = 1/2$ channel has not been reported yet, mainly because the rectangular diagram is exceptionally hard to rigorously calculate, the statistical error of the numerically computed K^* mass is not too small, and there are not enough theoretical formulas available to describe the πK system in the moving frame.

Motivated by the recent extensions and developments of the Rummukainen-Gottlieb formula [19] to a generic two-particle system with arbitrary masses in the moving frame [20–26] and Nebreda and Pelaez's brilliant expositions on the $K^*(892)$ resonance [27], and also encouraged by our previous work on the precise extraction of the K^* mass [28], the exploratory calculations of the scalar meson decay widths [21,29,30], and the reliable extraction of the πK scattering length in the $I = 1/2$ channel [31], we will further explore its decay width directly from lattice QCD simulations.

In the present work, we will obtain the $K^*(892)$ decay width by calculating the p-wave πK scattering phase shift in the $I = 1/2$ channel. We will discuss the energy eigenstates of the πK system with total zero momentum in the center-of-mass frame, and total nonzero momentum in the moving frame, respectively. The calculations are launched on a MILC gauge configuration with the $N_f = 2 + 1$ flavors of the Asqtad-improved staggered dynamical sea quarks [32,33]. The meson masses extracted from our previous spectrum analysis [28] yielded $(m_\pi + m_K)/m_{K^*} \approx 0.739$, and the lattice parameters were determined by the MILC collaboration, namely, the lattice extent L is about 3.0 fm and the lattice space inverse $1/a = 1.373$ GeV [32,33]. The Lüscher formula [34–36] is employed to study the πK system in the center-of-mass frame, and we utilize a newly established finite-size formula—which is the extension of the famous Rummukainen-Gottlieb formula [19] to the generic two-particle system in the moving frame [20–26]—to estimate the p-wave πK scattering phase shift in the $I = 1/2$ channel. These simulations are conducted at two energy

*fuziwen@scu.edu.cn
†gkanfu@gmail.com

eigenstates which allow us to examine the presence of the $K^*(892)$ resonance.

This paper is organized as follows. In Sec. II we elaborate on our calculation method. Our concrete lattice calculations are provided in Sec. III. We deliver our results in Sec. IV, and reach our conclusions and outlooks in Sec. V. Numerical calculations of the zeta function are courteously supplied in the Appendix for reference.

II. FORMALISM AND METHOD OF MEASUREMENT

A. The relativistic Breit-Wigner formula

The $K^*(892)$ resonance possesses quantum numbers $I(J^P) = \frac{1}{2}(1^-)$ and principally decays into one pion and one kaon in the p-wave with a branching rate of 99.9% [1]. In an elastic πK scattering, the relativistic Breit-Wigner formula for the p-wave scattering phase δ_1 in the resonance region with the center-of-mass energy M_R and a decay width Γ_R can be written as [1]

$$\tan\delta_1 = \frac{\sqrt{s}\Gamma_R(s)}{M_R^2 - s}, \qquad s = E_{\mathrm{CM}}^2, \tag{1}$$

where E_{CM} is the center-of-mass energy, and s is the Mandelstam variable or the invariant mass of the πK system. The decay width $\Gamma_R(s)$ can be expressed by way of the effective $K^* \to \pi K$ coupling constant $g_{K^*\pi K}$ as [27]

$$\Gamma_R(s) = \frac{g_{K^*\pi K}^2}{6\pi}\frac{p^3}{s}, \qquad p = \frac{1}{2\sqrt{s}}\sqrt{[s - (m_\pi - m_K)^2][s - (m_\pi + m_K)^2]}. \tag{2}$$

Combining Eqs. (1) and (2), a representation of the p-wave scattering phase as a function of the invariant mass $\sqrt{s}$ is offered by the effective range formula,

$$\tan\delta_1 = \frac{g_{K^*\pi K}^2}{6\pi}\frac{p^3}{\sqrt{s}(M_R^2 - s)}, \tag{3}$$

which suits the experimental measurements rather well, and permits us either a linear fit or to solve for the two unknown parameters: the coupling constant $g_{K^*\pi K}$ and the resonance position M_R from the scattering phase extracted through lattice QCD. The $K^*(892)$ decay width Γ_{K^*} can then be computed by

$$\Gamma_{K^*} = \Gamma_R(s)|_{s=M_R^2} = \frac{g_{K^*\pi K}^2}{6\pi}\frac{p_{K^*}^3}{M_R^2}, \qquad p_{K^*} = \frac{1}{2M_R}\sqrt{[M_R^2 - (m_\pi - m_K)^2][M_R^2 - (m_\pi + m_K)^2]}. \tag{4}$$

Thus, Eqs. (3) and (4) provide us with an approach to extracting the $K^*(892)$ decay width Γ_{K^*} through studying the dependence of the p-wave πK scattering phase shift δ_1 on the invariant mass $\sqrt{s}$. We should stress at this point that we will extensively use the effective range formula approximation in this work since the relativistic Breit-Wigner formula holds perfectly for relatively narrower objects and the $K^*(892)$ resonance has a rather narrow decay width of 50.8 ± 0.9 MeV [1].

B. Finite-volume methods

In the present study, we deliberate on the $K^*(892)$ meson decay into one pion and one kaon in the p-wave, and only focus on the πK system with the isospin representation of $(I, I_z) = (1/2, 1/2)$.

1. Center-of-mass frame

In the center-of-mass frame, when the $K^*(892)$ meson is at rest, the possible energy eigenvalues of the noninteracting πK system are provided by

$$E = \sqrt{m_\pi^2 + p^2} + \sqrt{m_K^2 + p^2},$$

where $p = |\mathbf{p}|$, $\mathbf{p} = (2\pi/L)\mathbf{n}$, and $\mathbf{n} \in \mathbb{Z}^3$. In a typical lattice investigation, this energy for $\mathbf{n} \neq 0$ is significantly bigger than the $K^*(892)$ resonance mass m_{K^*}. For example, in our concrete study, the lowest energy for $\mathbf{n} \neq 0$ calculated from the previous determination of m_π, m_K, and m_{K^*} [28] is $E = 1.12 \times m_{K^*}$, which is self-evidently not qualified to study the $K^*(892)$ decay. Hence, we have no choice but to consider the $\mathbf{n} = 0$ case, and the energy $E = 0.739 \times m_{K^*}$, which is still not a favorable option.

When considering the interaction of the πK system, the energy eigenstates are displaced by the hadronic interaction from E to $\bar{E}$, and the energy eigenvalue for the πK system can be written as

$$\bar{E} = \sqrt{m_\pi^2 + k^2} + \sqrt{m_K^2 + k^2}, \qquad k = \frac{2\pi}{L}q,$$

where $q \in \mathbb{R}$. Solving this equation for the scattering momentum k, we get

$$k = \frac{1}{2\bar{E}}\sqrt{[\bar{E}^2 - (m_\pi - m_K)^2][\bar{E}^2 - (m_\pi + m_K)^2]}.$$

In this article, we are primarily interested in the energy eigenstates of the πK system in the elastic region $m_\pi + m_K < \bar{E} < 2(m_\pi + m_K)$. In the center-of-mass frame these energy eigenstates transform as a vector (to be specific, the irreducible representation $\Gamma = T_1^+$) under the cubic group O_h. The Lüscher formula links the energy $\bar{E}$ to the p-wave πK scattering phase δ_1 [34–36], namely,

$$\tan\delta_1(k) = \frac{\pi^{3/2}q}{\mathcal{Z}_{00}(1; q^2)}, \tag{5}$$

where the zeta function is formally defined by

$$\mathcal{Z}_{00}(s; q^2) = \frac{1}{\sqrt{4\pi}}\sum_{\mathbf{n}\in\mathbb{Z}^3}\frac{1}{(|\mathbf{n}|^2 - q^2)^s}. \tag{6}$$

The $\mathcal{Z}_{00}(s;q^2)$ has a finite value only if $\mathrm{Re}s > 3/2$; nevertheless it could be analytically continued to $s = 1$. We usually evaluate $\mathcal{Z}_{00}(s;q^2)$ using the method described in Ref. [37]. We notice that there exists an equivalent Lüscher formula in Ref. [38], which is the generalization of the Lüscher quantization condition to multiple two-body channels. Moreover, it is easy to calculate and more accurate than the Lüscher formula in the relativistic case.

2. Moving frame

To implement the physical kinematics such that the energy of the πK system is rather close to the K^* meson mass, we can employ a moving frame (or laboratory frame) [19]. We have presented the detailed discussions of πK system in the moving frame in Ref. [30]; here we just review its essential parts.

Using a moving frame with total nonzero momentum $\mathbf{P} = (2\pi/L)\mathbf{d}$, $\mathbf{d} \in \mathbb{Z}^3$, the energy eigenvalues for the noninteracting πK system are given by

$$E_{\mathrm{MF}} = \sqrt{m_\pi^2 + p_1^2} + \sqrt{m_K^2 + p_2^2},$$

where $p_1 = |\mathbf{p}_1|$, $p_2 = |\mathbf{p}_2|$, and $\mathbf{p}_1$, $\mathbf{p}_2$ define the three-momenta of π and K, respectively, which meet the periodic boundary condition,

$$\mathbf{p}_1 = \frac{2\pi}{L}\mathbf{n}_1, \qquad \mathbf{p}_2 = \frac{2\pi}{L}\mathbf{n}_2, \qquad \mathbf{n}_1, \mathbf{n}_2 \in \mathbb{Z}^3,$$

and the total momentum $\mathbf{P}$ satisfies $\mathbf{P} = \mathbf{p}_1 + \mathbf{p}_2$.

In the moving frame, the center-of-mass is shifting with a velocity of $\mathbf{v} = \mathbf{P}/E_{\mathrm{MF}}$. Using the standard Lorentz transformation with a boost factor $\gamma = 1/\sqrt{1-\mathbf{v}^2}$, the E_{CM} can be calculated by

$$E_{\mathrm{CM}} = \gamma^{-1} E_{\mathrm{MF}} = \sqrt{m_\pi^2 + p^{*2}} + \sqrt{m_K^2 + p^{*2}},$$

where the total center-of-mass momentum disappears in the center-of-mass frame, namely,

$$p^* = |\mathbf{p}^*|, \qquad \mathbf{p}^* = \mathbf{p}_1^* = -\mathbf{p}_2^*,$$

where and whereafter we delimit the center-of-mass momenta with an asterisk (*). We can readily verify that the $\mathbf{p}^*$ are quantized to the values [30]

$$\mathbf{p}^* = \frac{2\pi}{L}\mathbf{r}, \qquad \mathbf{r} \in P_{\mathbf{d}},$$

where the set $P_{\mathbf{d}}$ is

$$P_{\mathbf{d}} = \left\{\mathbf{r} | \mathbf{r} = \vec{\gamma}^{-1}\left[\mathbf{n} + \frac{\mathbf{d}}{2}\cdot\left(1 + \frac{m_K^2 - m_\pi^2}{E_{\mathrm{CM}}^2}\right)\right], \mathbf{n} \in \mathbb{Z}^3\right\}, \tag{7}$$

where the boost factor operates in the direction of the velocity $\mathbf{v}$, and for the notational compactness we use the shorthand notation

$$\vec{\gamma}\mathbf{p} = \gamma\mathbf{p}_\parallel + \mathbf{p}_\perp, \qquad \vec{\gamma}^{-1}\mathbf{p} = \gamma^{-1}\mathbf{p}_\parallel + \mathbf{p}_\perp, \tag{8}$$

where $\mathbf{p}_\parallel$ and $\mathbf{p}_\perp$ are the ingredients of $\mathbf{p}$ parallel and perpendicular to the velocity $\mathbf{v}$, respectively, i.e.,

$$\mathbf{p}_\parallel = \frac{\mathbf{p}\cdot\mathbf{v}}{|\mathbf{v}|^2}\mathbf{v}, \qquad \mathbf{p}_\perp = \mathbf{p} - \mathbf{p}_\parallel.$$

Since the relativistic four-momentum squared is invariant, E_{CM} is connected to E_{MF} via the standard Lorentz transformation $E_{\mathrm{CM}}^2 = E_{\mathrm{MF}}^2 - \mathbf{P}^2$.

We are particularly interested in one moving frame: the pion is at rest, the kaon has momentum $\mathbf{p} = (2\pi/L)\mathbf{e}_3$ (namely, $\mathbf{d} = \mathbf{e}_3$), and the $K^*(892)$ meson has momentum $\mathbf{P} = \mathbf{p}$. For our concrete case, we found that its invariant mass is $\sqrt{s} = 0.8788 \times m_{K^*}$, which is significantly closer to m_{K^*} than that in the center-of-mass frame. Therefore, here we will only consider this case.

In the interacting case, $\bar{E}_{\mathrm{CM}}$ can be calculated by

$$\bar{E}_{\mathrm{CM}} = \sqrt{m_\pi^2 + k^2} + \sqrt{m_K^2 + k^2}, \qquad k = \frac{2\pi}{L}q,$$

where $q \in \mathbb{R}$. Solving this equation for the scattering momentum k, we have

$$k = \frac{1}{2\bar{E}}\sqrt{[\bar{E}_{\mathrm{CM}}^2 - (m_\pi - m_K)^2][\bar{E}_{\mathrm{CM}}^2 - (m_\pi + m_K)^2]}. \tag{9}$$

We prefer to rewrite Eq. (9) in an elegant form for later use:

$$k^2 = \frac{1}{4}\left(\bar{E}_{\mathrm{CM}} + \frac{m_\pi^2 - m_K^2}{\bar{E}_{\mathrm{CM}}}\right)^2 - m_\pi^2, \tag{10}$$

which is used to calculate the scattering momentum k and to investigate the lattice discretization effect.

The energy eigenstates of the πK system for our chosen moving frame transform under the tetragonal group C_{4v}. Only the irreducible representations A_1 and E are associated with the p-wave πK scattering states in a torus. We compute the energies related with the A_1 sector in the present study. The hadronic interaction displaces the energy eigenstates of the πK system from E to $\bar{E}$, and the energy eigenstates $\bar{E}$ are linked to the πK scattering phase shift δ_1 with the πK system's Rummukainen-Gottlieb formula [20,21,23], namely,

$$\tan\delta_1(k) = \frac{\gamma\pi^{3/2}q}{\mathcal{Z}_{00}^{\mathbf{d}}(1;q^2) + \frac{2}{\sqrt{5}}q^{-2}\mathcal{Z}_{20}^{\mathbf{d}}(1;q^2)}, \tag{11}$$

where we ignore the higher scattering phase shifts $\delta_l (l = 2, 3, 4, \ldots)$ [22], and the modified zeta functions are formally defined as

$$\begin{aligned}\mathcal{Z}_{00}^{\mathbf{d}}(s;q^2) &= \sum_{\mathbf{r}\in P_{\mathbf{d}}} \frac{1}{(|\mathbf{r}|^2 - q^2)^s},\\ \mathcal{Z}_{20}^{\mathbf{d}}(s;q^2) &= \sum_{\mathbf{r}\in P_{\mathbf{d}}} \frac{r^2 Y_{20}(\Omega_r)}{(r^2 - q^2)^s},\end{aligned} \tag{12}$$

where Ω_r represents the solid angle parameters (θ, ϕ) of $\mathbf{r}$ in spherical coordinates and the Y_{lm} are the standard

spherical harmonic functions, and the set $P_{\mathbf{d}}$ is denoted in Eq. (7). The k is the scattering momentum defined from the invariant mass $\sqrt{s}$ as $\sqrt{s} = \sqrt{k^2 + m_\pi^2} + \sqrt{k^2 + m_K^2}$. We elaborated the calculation method of $\mathcal{Z}_{00}^{\mathbf{d}}(1; q^2)$ in Appendix of Ref. [30], and we will give the calculation method of $\mathcal{Z}_{20}^{\mathbf{d}}(1; q^2)$ in the Appendix here, although there is a general calculation of the zeta function $\mathcal{Z}_{lm}^{\mathbf{d}}(s; q^2)$ in Refs. [21,22,38]. Equation (11) is employed to achieve the scattering phase shift from the energy eigenvalue measured by the lattice calculations.

C. Correlation matrix

To compute two energy eigenvalues, i.e., $\bar{E}_n$ $(n = 1, 2)$, we constitute a 2×2 matrix of the time correlation function,

$$C(t) = \begin{pmatrix} \langle 0|\mathcal{O}_{\pi K}^\dagger(t)\mathcal{O}_{\pi K}(0)|0\rangle & \langle 0|\mathcal{O}_{\pi K}^\dagger(t)\mathcal{O}_{K^*}(0)|0\rangle \\ \langle 0|\mathcal{O}_{K^*}^\dagger(t)\mathcal{O}_{\pi K}(0)|0\rangle & \langle 0|\mathcal{O}_{K^*}^\dagger(t)\mathcal{O}_{K^*}(0)|0\rangle \end{pmatrix}, \tag{13}$$

where $\mathcal{O}_{K^*}(t)$ is an interpolating operator for the vector $K^*(892)$ meson with the specified momentum $\mathbf{p} = (2\pi/L)\mathbf{e}_3$ (namely, $\mathbf{d} = \mathbf{e}_3$) and the polarization vector parallel to $\mathbf{p}$, and $\mathcal{O}_{\pi K}(t)$ is an interpolating operator for the πK system with the given momentum $\mathbf{p} = (2\pi/L)\mathbf{e}_3$. The interpolating operators $\mathcal{O}_{K^*}$ and $\mathcal{O}_{\pi K}$ employed in the present work are exactly the same as those in our previous studies [28,31], and the notations and conventions adopted here are also the same; nevertheless, to make this article self-contained, all the required definitions will be provided in the following.

1. πK sector

Here we use the original derivations and conventions [39–43] to review the necessary formulas for the lattice QCD calculation of the p-wave scattering phase shift of the πK system for the isospin $I = 1/2$ channel in a torus. Let us review the πK system of one Nambu-Goldstone pion with zero momentum and one Nambu-Goldstone kaon with momentum $\mathbf{p}$ in the Asqtad-improved staggered dynamical fermion formalism. Using the operators $\mathcal{O}_\pi(x_1)$, $\mathcal{O}_\pi(x_3)$ for pions at points x_1, x_3, and the operators $\mathcal{O}_K(x_2)$, $\mathcal{O}_K(x_4)$ for kaons at points x_2, x_4, respectively, with the pion and kaon interpolating field operators denoted by

$$\mathcal{O}_{\pi^+}(\mathbf{x}, t) = -\bar{d}(\mathbf{x}, t)\gamma_5 u(\mathbf{x}, t),$$
$$\mathcal{O}_{\pi^0}(\mathbf{x}, t) = \frac{1}{\sqrt{2}}[\bar{u}(\mathbf{x}, t)\gamma_5 u(\mathbf{x}, t) - \bar{d}(\mathbf{x}, t)\gamma_5 d(\mathbf{x}, t)],$$
$$\mathcal{O}_{K^0}(\mathbf{x}, t) = \bar{s}(\mathbf{x}, t)\gamma_5 d(\mathbf{x}, t),$$
$$\mathcal{O}_{K^+}(\mathbf{x}, t) = \bar{s}(\mathbf{x}, t)\gamma_5 u(\mathbf{x}, t),$$

we can then describe the πK four-point correlation functions as

$$C_{\pi K}(x_4, x_3, x_2, x_1) = \langle \mathcal{O}_K(x_4)\mathcal{O}_\pi(x_3)\mathcal{O}_K^\dagger(x_2)\mathcal{O}_\pi^\dagger(x_1)\rangle.$$

After summing over the spatial coordinates $\mathbf{x}_1$, $\mathbf{x}_2$, $\mathbf{x}_3$, and $\mathbf{x}_4$, we gain the πK four-point correlation function with momentum $\mathbf{p}$,

$$C_{\pi K}(\mathbf{p}; t_4, t_3, t_2, t_1) = \sum_{\mathbf{x}_1}\sum_{\mathbf{x}_2}\sum_{\mathbf{x}_3}\sum_{\mathbf{x}_4} e^{i\mathbf{p}\cdot(\mathbf{x}_4 - \mathbf{x}_2)} \times C_{\pi K}(x_4, x_3, x_2, x_1),$$

where $x_1 \equiv (\mathbf{x}_1, t_1)$, $x_2 \equiv (\mathbf{x}_2, t_2)$, $x_3 \equiv (\mathbf{x}_3, t_3)$, and $x_4 \equiv (\mathbf{x}_4, t_4)$, and t represents the time difference, i.e., $t \equiv t_3 - t_1$. To avoid the complicated Fierz rearrangement of the quark lines [41], we select $t_1 = 0$, $t_2 = 1$, $t_3 = t$, and $t_4 = t + 1$. We write the πK operator in the $I = 1/2$ channel as [43]

$$\mathcal{O}_{\pi K}^{I=\frac{1}{2}}(\mathbf{p}, t) = \frac{1}{\sqrt{3}}\Big\{\sqrt{2}\pi^+(t)K^0(\mathbf{p}, t+1) - \pi^0(t)K^+(\mathbf{p}, t+1)\Big\}, \tag{14}$$

where $\mathbf{p}$ is the total momentum of the πK system or the momentum of the K meson. This πK operator has the isospin representation of $(I, I_z) = (1/2, 1/2)$.

Assuming that u and d quarks have equal mass, only three quark line diagrams contribute to πK scattering amplitudes [43]. The quark line diagrams dedicated to the πK four-point correlation function are elucidated in Fig. 1, where they are labeled as direct diagram (D), crossed diagram (C), and rectangular diagram (R), respectively. The direct and crossed diagrams can be readily computed [40,41] by means of only two wall sources fixed at the time slices t_1 and t_2, which enables a relatively cheap lattice calculation of the $I = 3/2$ πK scattering length [44,45]. Nevertheless, the rectangular diagram (R) needs an additional quark propagator connecting the time slices t_3 and t_4, which causes the strict evaluation of this diagram to be extraordinarily expensive.

Sasaki *et al.* handled this problem, viz., the technique with a fixed kaon sink operator to reduce the computational resources [46]. Lang *et al.* recently solved it by the use of the Laplacian-Heaviside smeared quarks within the

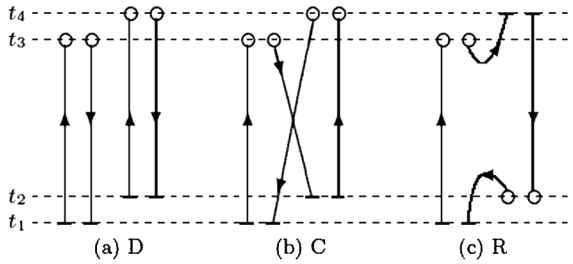

FIG. 1. Diagrams contributing to πK four-point functions. Short bars stand for wall sources. Open circles are sinks for local pion or kaon operators. The thicker lines represent the strange quark lines.

distillation method [47].[1] In our previous work [21], we settled this by using the moving wall sources without gauge fixing first introduced by Kuramashi *et al.* [40,41], namely, we calculated these diagrams by evaluating T quark propagators corresponding to the moving wall source at all of the time slices $t = 0, \cdots, T-1$ on a $L^3 \times T$ lattice, which is denoted as [40,41]

$$\sum_{n''} D_{n',n''} G_t(n'') = \sum_{\mathbf{x}} \delta_{n',(\mathbf{x},t)}, \qquad 0 \le t \le T-1,$$

where D is the Dirac quark matrix for the staggered Kogut-Susskind quark action, and the subscript t in the quark propagator G stands for the position of the wall source. The association of the quark propagators $G_t(n)$ which we use for the πK four-point functions is illustrated in Fig. 1. In practice, for the nonzero momentum we employ an up quark source with 1, and a strange quark source with $e^{i\mathbf{p}\cdot\mathbf{x}}$ on each site for the pion and kaon creation operator, respectively. D, C, and R, are schematically shown in Fig. 1, and we can represent them by means of the quark propagators G, namely,

$$\begin{aligned}
C^D_{\pi K}(\mathbf{p}; t_4, t_3, t_2, t_1) &= \sum_{\mathbf{x}_3}\sum_{\mathbf{x}_4} e^{i\mathbf{p}\cdot\mathbf{x}_4} \langle \mathrm{Tr}[G^\dagger_{t_1}(\mathbf{x}_3, t_3) G_{t_1}(\mathbf{x}_3, t_3)] \\
&\quad \times \mathrm{Tr}[G^\dagger_{t_2}(\mathbf{x}_4, t_4) G_{t_2}(\mathbf{x}_4, t_4)] \rangle, \\
C^C_{\pi K}(\mathbf{p}; t_4, t_3, t_2, t_1) &= \sum_{\mathbf{x}_3}\sum_{\mathbf{x}_4} e^{i\mathbf{p}\cdot\mathbf{x}_4} \langle \mathrm{Tr}[G^\dagger_{t_1}(\mathbf{x}_3, t_3) G_{t_2}(\mathbf{x}_3, t_3) \\
&\quad \times G^\dagger_{t_2}(\mathbf{x}_4, t_4) G_{t_1}(\mathbf{x}_4, t_4)] \rangle, \\
C^R_{\pi K}(\mathbf{p}; t_4, t_3, t_2, t_1) &= \sum_{\mathbf{x}_2}\sum_{\mathbf{x}_3} e^{i\mathbf{p}\cdot\mathbf{x}_2} \langle \mathrm{Tr}[G^\dagger_{t_1}(\mathbf{x}_2, t_2) G_{t_4}(\mathbf{x}_2, t_2) \\
&\quad \times G^\dagger_{t_4}(\mathbf{x}_3, t_3) G_{t_1}(\mathbf{x}_3, t_3)] \rangle,
\end{aligned}$$

where the traces are taken over color, and the Hermiticity properties of the propagator G have been applied to eliminate the γ^5 factors.

As discussed in Refs. [40,41], the rectangular diagram produces gauge-variant noise, and we reduce it, viz., by performing the gauge field average without gauge fixing, as we practiced in Refs. [21,30,48,49]. All three diagrams in Fig. 1 are needed to calculate the πK scattering in the $I = 1/2$ channel. As it is investigated in Ref. [43], in the isospin limit, the πK correlation function in the $I = 1/2$ channel is described in terms of only three diagrams, namely,

$$\begin{aligned}
C_{\pi K}(\mathbf{p}, t) &\equiv \langle \mathcal{O}_{\pi K}(\mathbf{p}, t) | \mathcal{O}_{\pi K}(\mathbf{0}, 0) \rangle \\
&= D + \frac{1}{2} N_f C - \frac{3}{2} N_f R,
\end{aligned} \tag{16}$$

where the operator $\mathcal{O}_{\pi K}$ denoted in Eq. (14) creates a πK state with total isospin $1/2$ and momentum $\mathbf{p}$. The staggered-flavor factor N_f is inserted to address the flavor degrees of freedom of the Kogut-Susskind staggered fermion [39]. We should keep in mind the fact that if we carry out the appropriate root of the staggered fermion determinant[2] in the continuum limit, the same number of flavors flow around internal quark loops as in QCD [39]. Therefore, at the level of the diagrams, all contributions are exactly as in QCD [39].

In our concrete calculation we also evaluate the ratios[3]

$$\begin{aligned}
R^X(t) &= \frac{C^X_{\pi K}(\mathbf{p}; 0, 1, t, t+1)}{C_\pi(\mathbf{0}; 0, t) C_K(\mathbf{p}; 1, t+1)}, \\
X &= D, C, \quad \text{and} \quad R,
\end{aligned} \tag{17}$$

where $C_\pi(\mathbf{0}; 0, t)$ and $C_K(\mathbf{p}; 1, t+1)$ are pion and kaon correlators with momentum $\mathbf{0}$ and $\mathbf{p}$, respectively.

We should bear in mind that the dedications of non-Nambu-Goldstone pions and non-Nambu-Goldstone kaons in the intermediate states are exponentially reduced for large times owing to their relatively heavier masses as compared to these of Nambu-Goldstone pions and Nambu-Goldstone kaons [39–41]. Thus, we can grant that the πK interpolator does not couple remarkably to other πK tastes, and ignore this systematic error.

2. $K^*(892)$ sector

In our previous work [28], we presented a detailed procedure to measure the K^* correlator $\langle 0|K^{*\dagger}(t) \times K^*(0)|0\rangle$. In principle, we can calculate the propagators for two local vector K^* mesons, $\gamma_i \otimes \gamma_i$ VT and $\gamma_0\gamma_i \otimes \gamma_0\gamma_i$ PV [60,61]. However, in this paper we simply quote the results for the local VT K^* meson since it delivers quite stable results in the analysis of the mass spectrum. Moreover, the numerical evaluation of the $K^* \to \pi K$ three-point function is much easier if we adopt the local VT K^* operator. Therefore, we employ an interpolation operator with the isospin $I = 1/2$ and $J^P = 1^-$ at the source and sink, namely,

$$\mathcal{O}(x) \equiv \sum_a u_a(x) \gamma_i \otimes \gamma_i \bar{s}_a(x),$$

[1] It is well-known that the rectangular diagram (or backtracking contractions, box diagram [47]) is most challenging and important for the $I = 1/2$ channel, and obtaining a reliable signal of it is vital to our final result. We observe that the signal of the rectangular diagram in Ref. [47] is at a reasonable level.

[2] There is some evidence demonstrating that conducting the fourth root of the fermion determinant recovers the contribution from a single Dirac fermion, see Ref. [50] for more details. In this work, we suppose that the fourth root trick reproduces the correct continuum limit of QCD, and the results of this work rely on this hypothesis. For the most recent discussions about the fourth-root trick, please see Refs. [51–59].

[3] If we impose the Dirichlet boundary condition in the temporal direction, we can easily extract the energy shift δE from the ratio R^X [40,41]. Moreover, we can readily check that when $t \ll T/2$, even if we choose the periodic boundary condition in the temporal direction, we can still roughly estimate δE from these ratios.

where a are the color indices, and we omit the Dirac spinor index. The time slice correlator for the K^* meson in the momentum $\mathbf{p}$ state can be evaluated as

$$C_{K^*}(\mathbf{p}, t) = \sum_{\mathbf{x}} \sum_{a,b} e^{i\mathbf{p}\cdot\mathbf{x}} \langle u_b(\mathbf{x}, t)\gamma_i \otimes \gamma_i \bar{s}_b(\mathbf{x}, t) s_a(\mathbf{0}, 0)\gamma_i \otimes \gamma_i \bar{u}_g^a(\mathbf{0}, 0)\rangle,$$

where $\mathbf{0}$, $\mathbf{x}$ are the spatial points of the K^* state at source and sink, respectively.

For staggered quarks, the meson propagators have the generic single-particle form

$$\mathcal{C}(t) = \sum_i A_i e^{-m_i t} + \sum_i A_i'(-1)^t e^{-m_i' t} + (t \to N_t - t),$$

where the oscillating terms correspond to particles with opposite parity. For the K^* meson correlator, we consider only one mass with each parity, and the oscillating parity partner is the p-wave meson with $J^P = 1^+$. The K_1 meson has $J^P = 1^+$, so it is the candidate for the oscillating parity partner of the vector K^* meson. However, these states with $J^P = 1^+$ can just as well be multihadron states [62]. With staggered fermions, the multihadron possibilities include the various taste combinations, so we cannot identify its parity partner with the K_1 (see more discussions in Ref. [28]). Thus, the $K^*(892)$ correlator was fit to the following physical model:

$$C_{K^*}(t) = b_{K^*} e^{-m_{K^*} t} + b_{K_1}(-1)^t e^{-M_{K_1} t} + (t \to N_t - t), \tag{18}$$

where b_{K_1} and b_{K^*} are two overlap factors.

3. Off-diagonal sector

A calculation of the generic three-point function is briefly discussed in Ref. [10]. To rigorously evaluate it we must compute a number of spatial volume propagators, namely N_L^3 (16^3 for our case). To avoid the apparent intractability of exactly computing this problem, Gottlieb *et al.* introduced the *exponential* method, which calculates a two-point function with the presence of a source and then differentiates with the source strength to achieve the corresponding three-point functions [7,8]. To investigate vector meson decay into pseudoscalars from quenched lattice QCD [10], Loft and DeGrand adopted a *two-stage* technique [63,64], which takes approximately twice as long as the calculation of the mass spectra [10]. Later, when studying the resonance parameter of the vector ρ meson [10–18], a stochastic method [65–67] or its variants are chiefly employed to evaluate the three-point correlation functions.

Motivated by the precise evaluation of the $\pi\pi$ four-point correlation functions by Kuramashi *et al.* [40,41] with the moving wall source technique [31], analogously, we have successfully extended this technique to evaluate the three-point correlation function, and have obtained rather good signals for the three-point functions of the $\pi\pi \to \sigma$ [29] and $\pi K \to \kappa$ [30]. In this work we will continue to use this technique to evaluate the $\pi K \to K^*$ three-point correlation function.

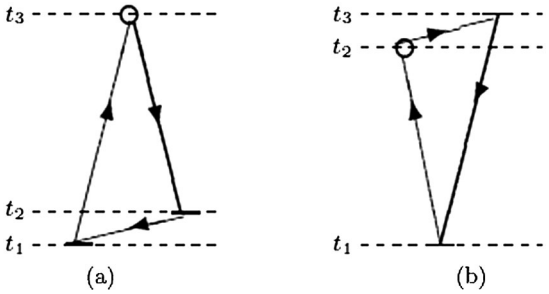

FIG. 2. Diagrams contributing to the $\pi K \to K^*$ and $K^* \to \pi K$ three-point functions. Short bars stand for the wall sources. The thicker lines represent the strange quark lines. (a) Quark contractions of $\pi K \to K^*$, where open circles are sinks for the local K^* operator. (b) Quark contractions of $K^* \to \pi K$, where open circles are sinks for the local pion operator.

To prevent the complicated color Fierz transformation of the quark lines [41], we choose $t_1 \neq t_2$. In practice, we pick $t_1 = 0$, $t_2 = 1$, and $t_3 = t$ for the $\pi K \to K^*$ three-point correlation function, and pick $t_1 = 0$, $t_2 = t$, and $t_3 = t + 1$ for the $K^* \to \pi K$ three-point function. The quark line diagrams corresponding to the $K^* \to \pi K$ and $\pi K \to K^*$ three-point functions are illustrated in Figs. 2(a) and 2(b), respectively.

The $\pi K \to K^*$ three-point function can be easily evaluated using only two wall sources [21,30]. Nevertheless, the evaluation of $K^* \to \pi K$ three-point function is hard, since it requires additional quark propagator connecting time slices t_2 and t_3. In practice, we employ an up quark source with 1 on each site for the pion creation operator, and a strange quark source with $e^{i\mathbf{p}\cdot\mathbf{x}}$ on each site for the kaon creation operator. The $K^* \to \pi K$ and $\pi K \to K^*$ three-point functions are schematically illustrated in Fig. 2, and we write them in terms of quark propagators G:

$$\begin{aligned} C_{\pi K \to K^*}(\mathbf{p}; t_3, t_2, t_1) &= \sum_{\mathbf{x}_3, \mathbf{x}_2} e^{i\mathbf{p}\cdot\mathbf{x}_3} \langle \mathrm{Tr}[G_{t_1}(\mathbf{x}_3, t_3)\gamma_5 \\ &\quad \times G_{t_2}^\dagger(\mathbf{x}_3, t_3)\gamma_3 G_{t_1}^\dagger(\mathbf{x}_2, t_2)]\gamma_5\rangle, \\ C_{K^* \to \pi K}(\mathbf{p}; t_3, t_2, t_1) &= \sum_{\mathbf{x}_2, \mathbf{x}_3} e^{i\mathbf{p}\cdot\mathbf{x}_2} \langle \mathrm{Tr}[G_{t_1}(\mathbf{x}_2, t_2)\gamma_3 \\ &\quad \times G_{t_3}^\dagger(\mathbf{x}_2, t_2)\gamma_5 G_{t_1}^\dagger(\mathbf{x}_3, t_3)]\gamma_5\rangle, \end{aligned} \tag{19}$$

where the trace is over the color index. The Dirac matrices are used as an interpolating field for the ith meson: γ_5 for pseudoscalars and γ_3 for the vector meson.

D. Extraction of energies

To map out *avoided level crossings* between the K^* resonance and its decay products (i.e., π and K), it is important to separate the ground state from the first excited

state by calculating the 2×2 correlation function matrix $C(t)$ denoted in Eq. (13). We apply the variational method [36] and construct a ratio of the correlation function matrices as

$$M(t, t_R) = C(t)C^{-1}(t_R), \tag{20}$$

with some reference time t_R [36] to extract the two lowest energy eigenvalues $\bar{E}_n$ ($n = 1, 2$), which can be obtained by a cosh-fit to two eigenvalues $\lambda_n(t, t_R)$ ($n = 1, 2$) of the correlation matrix $M(t, t_R)$. Considering the use of the staggered fermion, it is easy to verify explicitly that $\lambda_n(t, t_R)$ ($n = 1, 2$) has an oscillating term [68–70], namely,

$$\lambda_n(t, t_R) = A_n \cosh\left[-E_n\left(t - \frac{T}{2}\right)\right] + (-1)^t B_n \cosh\left[-E'_n\left(t - \frac{T}{2}\right)\right], \tag{21}$$

for a large t, which means that $0 \ll t_R < t \ll T/2$ to suppress both the excited states and the wrap-around contributions [30,71–73].[4] Without loss of generality, we suppose $\lambda_1(t, t_R) > \lambda_2(t, t_R)$.

III. LATTICE CALCULATION

A. Simulation parameters

We use the MILC gauge configurations in the presence of the $N_f = 2 + 1$ dynamical flavors of the Asqtad-improved staggered dynamical fermions [60,61] and a Symanzik-improved gluon action [74]: a detailed description of the simulation parameters can be found in Refs. [32,33]. We should keep in mind that the MILC gauge configurations are generated using the staggered formulation of lattice fermions [75] with the fourth root of the fermion determinant [60].

We measured the πK four-point correlation functions on the 0.15 fm MILC *medium* coarse lattice ensemble of 400 $20^3 \times 48$ gauge configurations with the bare quark masses $am_{ud} = 0.00484$ and $am_s = 0.0484$ and bare gauge coupling $10/g^2 = 6.566$, which has a physical volume of approximately 3.0 fm. The inverse lattice spacing $a^{-1} = 1.373^{+34}_{-14}$ GeV [32,33]. The mass of the dynamical strange quark is quite close to its physical value, and the masses of the u and d quarks are degenerate. Periodic boundary conditions are imposed on three spatial directions and the temporal direction.

B. Computations

To compute the πK four-point functions, we employ the standard conjugate gradient method to achieve the necessary matrix element of the inverse Dirac fermion matrix. We compute the correlators on all the time slices, and explicitly combine the results from each of the $N_T = 48$ time slices, namely, the diagonal correlator $C_{11}(t)$ is measured through

$$C_{11}(t) = \langle(\pi K)(t)(\pi K)^\dagger(0)\rangle = \frac{1}{T}\sum_{t_s}\langle(\pi K)(t + t_s)(\pi K)^\dagger(t_s)\rangle.$$

After averaging the propagator over all $N_T = 48$ possible values, we find that the statistics are significantly improved.

For each time slice, six fermion matrix inversions are required corresponding to the three possible color choices for the pion source and kaon source, respectively. Therefore, we perform a total of 288 inversions on each gauge configuration. This large number of matrix inversions, carried out on 400 gauge configurations, provides the gigantic statistics required to reliably calculate the πK four-point functions.

For the diagonal correlator $C_{22}(t)$, the $K^*(892)$ correlator, we have produced the point-to-point correlators with high accuracy in our previous study [28]. Therefore, we can simply exploit these calculated propagators to calculate the $K^*(892)$ correlator:

$$C_{22}(t) = \frac{1}{T}\sum_{t_s}\langle K^{*\dagger}(t + t_s)K^*(t_s)\rangle,$$

where, again, we sum the correlator over all the time slices t_s and take the average.

We evaluate the first off-diagonal correlator $C_{21}(t)$ through

$$C_{21}(t) = \langle K^*(t)(\pi K)^\dagger(0)\rangle = \frac{1}{T}\sum_{t_s}\langle K^*(t + t_s)(\pi K)^\dagger(t_s)\rangle,$$

where the summation is over all time slices t_s. Through the relation $C_{12}(t) = C^*_{21}(t)$ we can gratuitously gain the second off-diagonal correlator $C_{12}(t)$.

In the present study, we evaluate the two-point correlation functions for the pion and kaon as well, namely,

$$G_\pi(\mathbf{0}; t) = \frac{1}{T}\sum_{t_s}\langle 0|\pi^\dagger(\mathbf{0}, t + t_s)\pi(\mathbf{0}, t_s)|0\rangle,$$
$$G_K(\mathbf{p}; t) = \frac{1}{T}\sum_{t_s}\langle 0|K^\dagger(\mathbf{p}, t + t_s)K(\mathbf{p}, t_s)|0\rangle, \tag{22}$$

where $G_\pi(\mathbf{0}; t)$ is the two-point correlation function for the pion meson with zero momentum, and $G_K(\mathbf{p}; t)$ is the propagator for the kaon meson with momentum $\mathbf{p}$.

IV. SIMULATION RESULTS

In our previous work [28], we measured the point-to-point pion and kaon correlators with high accuracy.

[4] In Ref. [30] we gave a detailed discussion about a contamination from *wraparound* effects. In practice, we will select the fitting time ranges satisfying $t_{\max} \leq 16$, and reasonably neglect it.

TABLE I. Masses m of pion, kaon, and $K^*(892)$ mesons, and energies E of kaon and $K^*(892)$ mesons with momentum $\mathbf{p} = (2\pi/L)\mathbf{e}_3$, extracted from the corresponding time correlation functions.

	π	K	$K^*(892)$
am	0.17503(17)	0.39913(27)	0.7757(70)
aE		0.50465(48)	0.8278(82)

Exploiting these correlators, we can reliably extract the pion mass (m_π) and kaon mass (m_K), which are in fair agreement with the previous MILC determinations in Ref. [33]. In Table I we list the pion mass m_π, the mass m_K, and the energy E_K of the kaon meson with momentum $\mathbf{p} = (2\pi/L)\mathbf{e}_3$, which are extracted through a single exponential fit to $G_\pi(t;\mathbf{0})$ and $G_K(t;\mathbf{p})$ in Eq. (22). We also show the mass and energy of the vector $K^*(892)$ meson with momentum $\mathbf{p} = (2\pi/L)\mathbf{e}_3$, which are calculated from the $K^*(892)$ correlator.

We must stress at this point that, in this work, we just use the calculated $K^*(892)$ mass m_{K^*} to indicate the position of the free $K^*(892)$ mass.

A. Diagrams *D*, *C*, and *R*

In Fig. 3 the individual ratios R^X ($X = D$, C and R), which correspond to the diagrams in Fig. 1, are illustrated as functions of t. We can see that diagram D has the biggest contribution, followed by diagram C and diagram R. Clear signals observed up to $t = 20$ for the rectangular amplitude demonstrate that the technique of the moving wall source without gauge fixing used here is practically applicable.

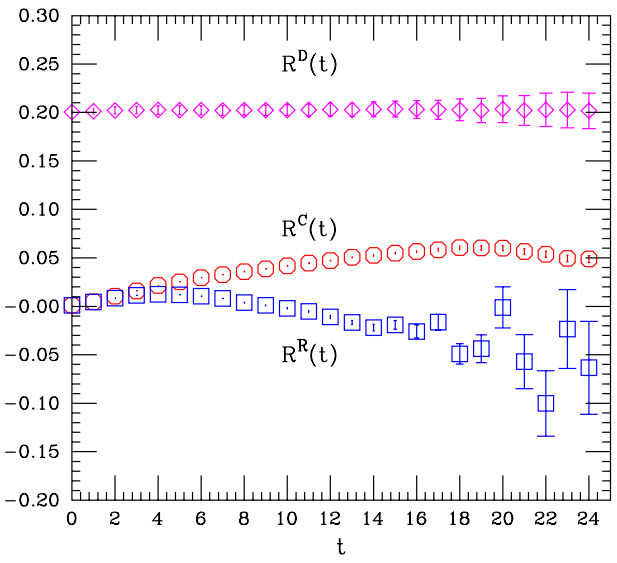

FIG. 3 (color online). Individual amplitude ratios $R^X(t)$ for the πK four-point function evaluated by the moving wall source without gauge fixing as functions of t. Direct diagram (magenta diamonds) shifted by 0.8, crossed diagram (red octagons) and rectangular diagram (blue squares).

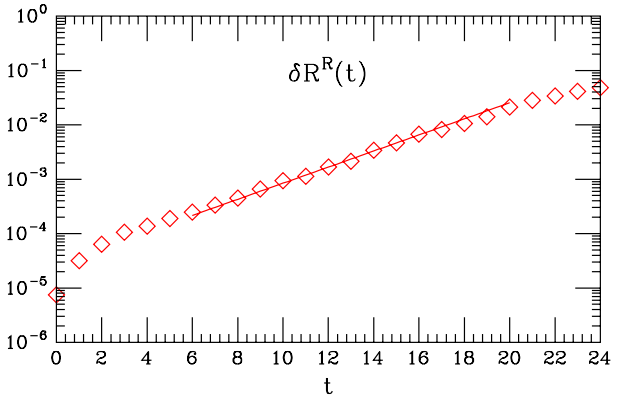

FIG. 4 (color online). The error of the ratio $R^R(t)$ as a function of time slice t. The solid lines are single exponential fits over the range $10 \le t \le 16$.

The values of the direct amplitude R^D are rather close to unity, indicating that the interaction in this channel is quite weak. The crossed amplitude R^C, on the other hand, increases linearly, implying a repulsion in this channel. After a starting increase up to $t \sim 4$, the rectangular amplitude R^R demonstrates a roughly linear decrease up until $t \sim 15$, and loss of signals after that, suggesting an attractive force between the pion and kaon. These characteristics are what we expected from the theoretical predictions [39,76]. We can observe that the crossed and rectangular amplitudes take the same value at $t = 0$, and similar values for small t. Since our analytical representations for both amplitudes are identical at this value of t, they should manifest analogously until the asymptotic πK state is reached.

According to the analytical arguments in Ref. [77], we can infer that the ratio for the rectangular diagram R^R has errors, which should increase exponentially as $e^{m_K t}$ for large time separation. The magnitude of the errors is in quantitative agreement with this theoretical prediction, as displayed in Fig. 4. Fitting the errors $\delta R^R(t)$ by a single exponential fit ansatz $\delta R^R(t) \sim \exp(\mu_R t)$ over the range $10 \le t \le 16$, we can achieve the corresponding fitting values of μ_R with $a\mu_R = 0.358$, which can be reasonably compared with the corresponding kaon masses m_K determined in our previous work [28] and also listed in Table I. This demonstrates, on the other hand, that the technique of the moving wall source without gauge fixing used in this work is practically feasible.

B. Energy eigenvalues

We calculate two eigenvalues $\lambda_n(t, t_R)$ ($n = 1, 2$) for the matrix $M(t, t_R)$ denoted in Eq. (20) with the reference time $t_R = 5$. In Fig. 5 we illustrate our lattice simulation results for $\lambda_n(t, t_R)$ ($n = 1, 2$) on a logarithmic scale as a function of time t along with a correlated fit to the asymptotic form

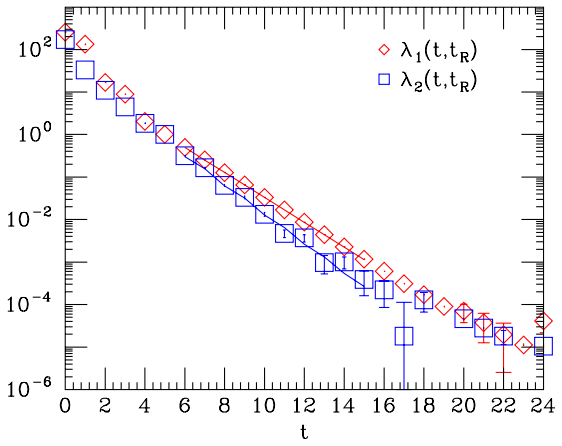

FIG. 5 (color online). The eigenvalues $\lambda_1(t, t_R)$ and $\lambda_2(t, t_R)$. Occasional points with negative central values for the eigenvalue $\lambda_2(t, t_R)$ are not plotted. The solid lines are correlated fits to Eq. (21), from which the energy eigenvalues $\bar{E}_n$ $(n = 1, 2)$ are extracted. The lower curve $(n = 2)$ is slightly steeper than the upper curve $(n = 1)$.

offered in Eq. (21). From these fits we can then obtain the desired energies $\bar{E}_n$ $(n = 1, 2)$ which will be employed to extract the p-wave scattering phase shifts.

As we noticed in Refs. [29–31], we realize that properly extracting the energy eigenvalues is vital to our final conclusions. Since the Periodic boundary condition is imposed on three spatial directions and the temporal direction, we should suppress the wraparound contaminations [11,31]. By defining a fitting range $[t_{\rm min}, t_{\rm max}]$ and varying the values of the minimum fitting distance $t_{\rm min}$ and the maximum fitting distance $t_{\rm max}$, we obtain these energies in a correct manner. In practice, we make $t_{\rm min} = t_R + 1$ and increase the reference time t_R to reduce the excited contaminations [11]. Moreover, we choose $t_{\rm max}$ to be away from the time slice $T/2$ to reduce the wraparound effects [11]. Furthermore, we extract two eigenvalues $\lambda_n (n = 1, 2)$ with the *effective energy* plots, a variant of the effective mass plots, and they are fit to Eq. (21) by changing $t_{\rm min}$, and with $t_{\rm max}$ at either 15 or where the fractional statistical errors exceeded about 20% for two successive time slices. The effective energy plots as a function of $t_{\rm min}$ are illustrated in Fig. 6.

The energy eigenvalues $\bar{E}_n (n = 1, 2)$ were chosen by looking for the combination of a *plateau* in the effective energy plots as functions of $t_{\rm min}$ and a reasonable fit quality. We observed that the effective energies show only relatively small errors within a minimum time distance region $5 \le t_{\rm min} \le 8$ for $\bar{E}_1$ and $5 \le t_{\rm min} \le 6$ for $\bar{E}_2$, respectively. The fit quality χ^2/dof of the fitting parameters t_R, $t_{\rm min}$, and $t_{\rm max}$ along with the fitted numbers for $\bar{E}_n$ $(n = 1, 2)$ are summarized in Table II.

The energy of the pion and kaon in the noninteracting case (namely, E_1) is computed from the pion mass m_π and the kaon energy E_K listed in Table I as $E_1 = m_\pi + E_K$. This number is listed in the upper part of Table III. We

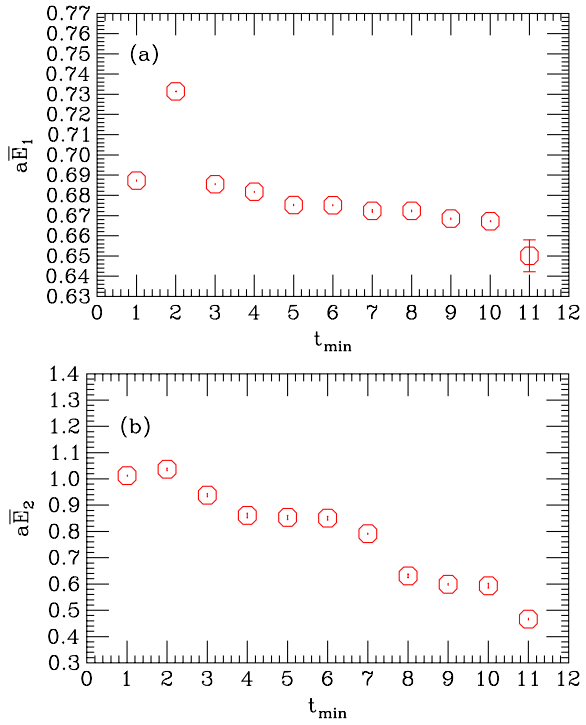

FIG. 6 (color online). The effective energy plots, $a\bar{E}_n$ $(n = 1, 2)$, as functions of $t_{\rm min}$. (a) The effective energy plot for $\bar{E}_1$ and (b) that for $\bar{E}_2$.

distinctly observe that $\bar{E}_1 < E_1 < \bar{E}_2$, which means that the phase shift for $\lambda_1(t, t_R)$ and $\lambda_2(t, t_R)$ is positive and negative, respectively. This evidently reveals the presence of a resonance between them.

C. Finite-size effects

We should pay attention to discretization error inherent in the πK system's Rummukainen-Gottlieb formula (11). This stems from the Lorentz transformation from the moving frame to the center-of-mass frame. When applying the Lorentz symmetry in the continuum limit, we utilize the relations [21,30]

$$\sqrt{s} = \sqrt{E_{\rm MF}^2 - p^2}, \quad k^2 = \frac{1}{4}\left(\sqrt{s} + \frac{m_\pi^2 - m_K^2}{\sqrt{s}}\right)^2 - m_\pi^2, \qquad (23)$$

in the Lorentz transformation for the invariant mass $\sqrt{s}$, the energy of the πK system in the moving frame $E_{\rm MF}$, and the

TABLE II. The fitted values of the energy eigenvalues for the ground state $(n = 1)$ and the first excited state $(n = 2)$. Here we tabulate the reference time t_R, the lower and upper bound of the fitting range, $t_{\rm min}$ and $t_{\rm max}$, the number of degrees of freedom (dof) for the fit quality χ^2/dof, and the fitted results for the energy eigenvalues $\bar{E}_n$ $(n = 1, 2)$ in lattice units.

n	t_R	$t_{\rm min}$	$t_{\rm max}$	$a\bar{E}_n$	χ^2/dof
1	5	6	15	0.67507(40)	12.2/6
2	5	6	15	0.8534(78)	9.6/6

TABLE III. Summary of the energy eigenvalues $\bar{E}_n$ ($n = 1, 2$) and p-wave scattering phase shift δ_1 for the πK system in a torus. E_1 is the energy of the free pion-kaon system. $\bar{E}_n (n = 1, 2)$ is obtained from fitting to eigenvalues $\lambda_n(t, t_R)$ ($n = 1, 2$). The invariant mass $\sqrt{s}$, the scattering momentum k, and the p-wave scattering phase shift δ_1 extracted through the energy-momentum expression (23) in the continuum are regarded as *Cont*, and those achieved with Eq. (24) on the lattice are regarded as *Lat*. The scattering momentum k_0 is denoted by $k_0^2 = 1/4 \times (\sqrt{s} + (m_\pi^2 - m_K^2)/\sqrt{s})^2 - m_\pi^2$. All values with the mass dimension are in lattice units.

	$n = 1$		$n = 2$	
E_n	0.67968(51)		—	
$\bar{E}_n$	0.67507(40)		0.8534(78)	
	Cont	Lat	Cont	Lat
$\sqrt{s}$	0.59751(45)	0.60350(45)	0.7934(84)	0.8004(84)
k^2	0.00588(13)	0.00750(14)	0.0690(30)	0.0729(31)
k_0^2	—	0.00745(13)	—	0.0717(30)
$\tan\delta_1$	0.0294(93)	0.0091(22)	−2.01(43)	−2.48(63)
$\sin^2\delta_1$	0.00087(55)	0.000083(39)	0.802(68)	0.860(62)

scattering momentum k. Nevertheless, on the lattice the discretization effects definitely violate the Lorentz symmetry and Eq. (23) is only effective up to the discretization errors.

Following the recommendations in Ref. [30], we calculate the invariant mass $\sqrt{s}$ and the scattering momentum k from the energy in the moving frame $E_{\rm MF}$ of πK system using

$$\cosh(\sqrt{s}) = \cosh(E_{\rm MF}) - 2\sin^2\left(\frac{p}{2}\right),$$
$$2\sin^2(k/2) = \cosh\left(\frac{\sqrt{s}}{2} + \frac{m_\pi^2 - m_K^2}{2\sqrt{s}}\right) - \cosh(m_\pi), \quad (24)$$

and then evaluate the p-wave scattering phase shift δ_1 by inserting the scattering momentum k into the finite-size formula in Eq. (11).

To grasp these discretization effects, in the present study we compute the invariant mass $\sqrt{s}$ and the scattering momentum k from the energy-momentum relations both in the continuum (23) and on the lattice (24), and then extract the p-wave scattering phase shift δ_1 by inserting the scattering momentum k into Eq. (11). We view the disparity stemming from the two options of the energy-momentum relations as the discretization error, which is expected to disappear in the continuum limit. The results for the invariant mass $\sqrt{s}$, the scattering momentum k, and the p-wave scattering phase shift δ_1 are summarized in Table III.

D. Extraction of the scattering phase shift and decay width

From Table III, the noticeable differences due to the two options of the energy-momentum relations are obviously

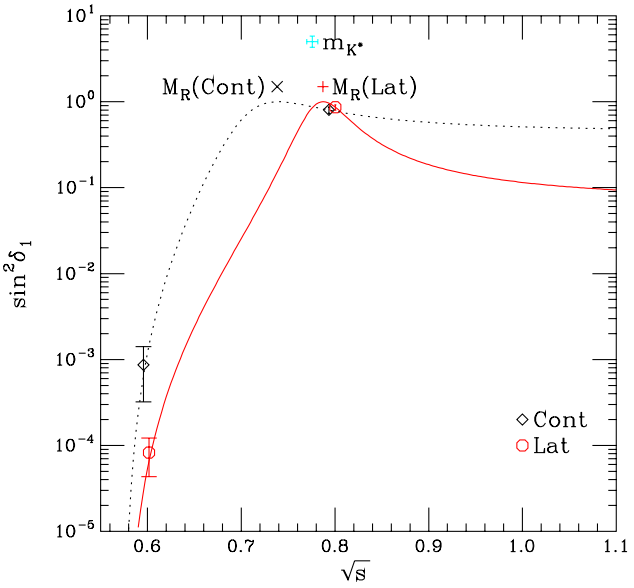

FIG. 7 (color online). The scattering phase $\sin^2\delta_1$, positions of m_{K^*}, and resonance mass M_R. *Cont* refer to the results achieved with energy-momentum expressions in the continuum (23) and *Lat* to those with relations on the lattice (24). The two lines are obtained by Eq. (25) with parameters $g_{K^*\pi K}$ and M_R given in Eqs. (26) and (27), respectively. The abscissa is in lattice units.

observed in $\sqrt{s}$ and k. Moreover, the differences for the p-wave scattering phase shift δ_1 due to the lattice discretization effects can be comparable with the statistical errors, and even considerably larger than its statistical error for the $n = 1$ case. These characteristics are also revealed in Fig. 7, where the p-wave scattering phase shift $\sin^2\delta_1$ is displayed. In Table III, we see that the sign of the p-wave scattering phase shift δ_1 at $\sqrt{s} < m_{K^*}$ [$am_{K^*} = 0.7757(70)$] is positive, indicating an attractive interaction, and that at $\sqrt{s} > m_{K^*}$ it is negative, suggesting a repulsive interaction. These features are what we expected. It verifies that there exists a resonance around the $K^*(892)$ mass m_{K^*}.

In principle, it is foolproof work to extract the $K^*(892)$ meson decay width through fitting the p-wave scattering phase shift data with the effective range formula since the kinematic factor in the decay width clearly depends on the quark mass [27]. Moveover, the quark mass we studied here is larger than its natural value; therefore, an extrapolation is indispensable. Nevertheless, in the present work, because of our limited computational resources, we simply made a lattice simulation on one set of the quark mass; therefore, we have no choice but to adopt an alternative method. As we explained in Sec. II A, we parameterize the resonant characteristic of the p-wave scattering phase shift δ_1 with the coupling constant $g_{K^*\pi K}$, namely,

$$\tan\delta_1 = \frac{g_{K^*\pi K}^2}{6\pi} \frac{k^3}{\sqrt{s}(M_R^2 - s)}, \quad (25)$$

where M_R is the resonance mass.

According to the elaborations in Refs. [27,78], we can suppose that the coupling constant $g_{K^*\pi K}$ varies quite slowly with the changing quark mass. Therefore, Eq. (25) enables us to solve for two unknown parameters, namely, the coupling constant $g_{K^*\pi K}$, and the resonance mass M_R.

The invariant mass $\sqrt{s}$ and the scattering momentum k appearing in Eq. (25) satisfy the energy-momentum relations (23). Hence, the discretization error may arise from the choice of $\sqrt{s}$ and k in the application of Eq. (25) to the p-wave scattering phase shift extracted from lattice QCD. Luckily, our lattice simulation results demonstrate that this does not cause a serious numerical problem. In Table III we also provide the scattering momentum k_0 calculated by $k_0^2 = 1/4 \times (\sqrt{s} + (m_\pi^2 - m_K^2)/\sqrt{s})^2 - m_\pi^2$. We can observe that the difference between k and k_0 is not significant, and we can neglect this systemic error for the present study. In practice, we employ the scattering momentum k_0 when applying Eq. (25).

The lattice simulation results of the coupling constant $g_{K^*\pi K}$ and the resonance mass M_R solved by Eq. (25) are

$$g_{K^*\pi K} = 11.73 \pm 2.08, \qquad M_R = 0.739(20), \qquad M_R/m_{K^*} = 0.953(28), \tag{26}$$

where we utilize the energy-momentum relations (23) in the continuum, and the K^* meson mass m_{K^*} is obtained from our previous study [28]. If we adopt the energy-momentum relations (24) on the lattice, we arive the simulation results

$$g_{K^*\pi K} = 6.38(78), \qquad M_R = 0.7873(97), \qquad M_R/m_{K^*} = 1.015(16). \tag{27}$$

The obtained value of the coupling constant $g_{K^*\pi K}$ is in reasonable agreement with $g_{K^*\pi K} \approx 5.5$, which is obtained from the residue of the amplitude at the pole position in Ref. [27]. Moreover, it is in reasonable agreement with the experimentally observed $g_{K^*\pi K} = 5.64(35)$ evaluated from the experimental results of the decay width $\Gamma_{K*} = 50.8(9)$ MeV [1] within the statistical error.

In Fig. 7, we illustrate the curves for $\sin^2\delta_1$ achieved by Eq. (25) with the coupling constant $g_{K^*\pi K}$ and the resonance mass M_R provided in Eqs. (26) and (27), respectively. The positions at $\sin^2\delta_1 = 1$, which represent the resonance mass M_R, are also marked in Fig. 7 for the two cases (black cross and red plus for the continuum and lattice case, respectively). For visual comparison, we also mark the $K^*(892)$ mass m_{K^*} with a cyan plus. We can observe that M_R is in reasonable accordance with the $K^*(892)$ mass m_{K^*}.

Assuming that the dependence of $g_{K^*\pi K}$ on the quark mass is small [27,78], we can roughly estimate the $K^*(892)$ meson decay width at the physical quark mass as

$$\Gamma^{\rm phy} = \frac{g_{K^*\pi K}^2}{6\pi} \frac{(k^{\rm phy})^3}{(m_{K^*}^{\rm phy})^2}, \tag{28}$$

where $m_{K^*}^{\rm phy} = 891.66(26)$ MeV is the physical $K^*(892)$ meson mass, which we take from the most recent Particle Data Group (PDG) findings [1], and the scattering momentum $k^{\rm phy}$ is calculated by

$$(k^{\rm phy})^2 = \frac{1}{4}\left(m_{K^*}^{\rm phy} + \frac{(m_\pi^{\rm phy})^2 - (m_K^{\rm phy})^2}{m_{K^*}^{\rm phy}}\right)^2 - (m_\pi^{\rm phy})^2,$$

where $m_\pi^{\rm phy}$ is physical pion mass ($m_\pi^{\rm phy} = 139.57018(35)$ MeV) [1], and $m_K^{\rm phy}$ is the physical kaon mass ($m_K^{\rm phy} = 493.677(13)$ MeV) [1]. This produces

$$\Gamma^{\rm phy} = (219 \pm 39) \text{ MeV}, \tag{29}$$

where we utilize the data given in Eq. (26), and

$$\Gamma^{\rm phy} = (64.9 \pm 8.0) \text{ MeV}, \tag{30}$$

where we use the data given in Eq. (27). The estimate in the lattice case in Eq. (30) is in fair agreement with the corresponding PDG data for the $K^* \to \pi K$ decay width, $\Gamma_{K^*} = 50.8 \pm 0.9$ MeV. We can observe that the difference stemming from our two options of the energy-momentum relations is much larger than the statistical error.

This is quite an encouraging result, considering that we make the assumption that the coupling constant $g_{K^*\pi K}$ does not depend on the quark mass, and that we performed an extrapolation, etc. One thing that greatly comforts us is that we use the pion mass (about 240 MeV), which is rather close to its realistic value (about 140 MeV), so we do not carry out a long extrapolation.

V. CONCLUSIONS AND OUTLOOKS

In the present work, we have carried out a direct lattice QCD computation of the p-wave πK scattering phase shift in the $I = 1/2$ channel near the $K^*(892)$ resonance region with total nonzero momentum in the moving frame, where the rectangular graph plays a vital role, for the MILC *medium* coarse ($a \approx 0.15$ fm) lattice ensemble in the presence of the $N_f = 2 + 1$ flavors of the Asqtad-improved staggered dynamical sea quarks. We employed the technique with the moving wall source without gauge fixing [31] introduced by Kuramashi *et al.* in Refs. [40,41] to calculate all three of the diagrams classified in Ref. [43] with high precision, and observed a clear signal of the attraction for the $I = 1/2$ channel.

We have exhibited that the lattice calculation of the p-wave scattering phase shifts for the $I = 1/2$ πK system and the estimation of the decay width of the $K^*(892)$ meson are feasible with our present limited computing resources. The phase shift data clearly reveals the presence of a resonance at a mass around the $K^*(892)$ meson mass obtained in our previous study [28]. This resonance can be reasonably identified with the $K^*(892)$ meson. Moreover, we extracted the $K^*(892)$ meson decay width from the phase shift data and showed that it is reasonably

comparable with the $K^*(892)$ meson decay reported by the PDG within the statistical error.

We have adopted the effective range formula, which allows us to exploit the effective $K^* \to \pi K$ coupling constant $g_{K^*\pi K}$ to extrapolate from our lattice simulation point $(m_\pi + m_K)/m_{K^*} = 0.7388$ to the physical point $(m_\pi + m_K)/m_{K^*} = 0.7102$, assuming that the coupling constant $g_{K^*\pi K}$ does not depend on the quark mass. This is just an approximate calculation, and therefore a more reliable computation of the decay width is highly desirable. As we pointed out above, the decay width can be estimated directly from the energy dependence of the phase shift data by fitting the BWRF if we make the lattice simulations near the physical quark mass and obtain simulation data which have several energies near the resonance mass. We will keep on enthusiastically requesting for the possible computational allocations to fulfil this valuable work.

Nevertheless, we should bear firmly in mind that some critical issues should be resolved in the more sophisticated calculation. One is to reduce the discretization errors, which, as we illustrated in the previous section, are significantly larger than the corresponding statistical errors. A naive way of handling this question is to utilize a lattice gauge configuration closer to the continuum limit. Another challenging and stimulating topic is to suppress the contaminations of the p-wave scattering phase from the d-wave scattering phase or higher, which we preliminarily touched on for the πK system in Ref. [21] (see more valuable discussions in Ref. [22]). Moreover, a comprehensive analysis to determine the lattice size dependence of the phase shift by employing a set of lattice sizes is highly desired. Nevertheless, all of these open questions are beyond the scope of this paper since this will demand a huge amount of computing allocations. We postpone these expensive tasks for our future study.

This work concentrated mainly on the scattering phase at two energies for a single lattice ensemble. Since, in this approach, we had only a small number of energies at hand, it becomes quite difficult to reliably map out the resonance region. Therefore, when our preliminary lattice results are compared with the experimentally measured quantities, it is obvious that the lattice QCD simulations can not yet match the experimental accuracy. Although a reliable extraction of the $K^*(892)$ resonance parameters from the lattice is quite challenging and most prospective, our rudimentary work reported here can still be viewed as an important conceptual study, and the techniques employed here will be useful for other resonances, such as the D^*, and possibly even for some exotic hadrons.

ACKNOWLEDGMENTS

We deeply appreciate the MILC Collaboration for supplying us with the Asqtad lattice ensemble and MILC codes. We should thank NERSC (National Energy Research Scientific Center) for providing us with the platform to download MILC gauge configurations and Massimo Di Pierro for his Python tool. The authors thank Carleton DeTar for his encouraging and critical comments and for supplying us with the fitting software. We especially thank Eulogio Oset for his enlightening and constructive comments and corrections. We are grateful to Hou Qing for his support. Numerical calculations for this paper were carried out at AMAX, CENTOS, and HP workstations in the Institute of Nuclear Science and Technology, Sichuan University.

APPENDIX: THE NUMERICAL EVALUATION OF THE $\mathcal{Z}^{\mathbf{d}}_{20}(1; q^2)$ FUNCTION

In this appendix we provide one simple approach for the numerical evaluation of the zeta function $\mathcal{Z}^{\mathbf{d}}_{20}(s; q^2)$ defined in Eq. (12) in the moving frame for any value of q^2. Here we follow the original derivations and notations in Refs. [22,30,37].

The definition of the zeta function $\mathcal{Z}^{\mathbf{d}}_{20}(s; q^2)$ in Eq. (12) is

$$\mathcal{Z}^{\mathbf{d}}_{20}(s; q^2) = \sum_{\mathbf{r}\in P_{\mathbf{d}}} \frac{\mathcal{Y}_{20}(\mathbf{r})}{(r^2 - q^2)^s}, \tag{A1}$$

where $\mathcal{Y}_{lm}(\mathbf{r}) \equiv r^l Y_{lm}(\Omega_r)$. Ω_r represents the solid angles (θ, ϕ) of $\mathbf{r}$ in spherical coordinates and the Y_{lm} are the spherical harmonic functions, and the summation for $\mathbf{r}$ is taken over the set

$$P_{\mathbf{d}} = \left\{\mathbf{r} | \mathbf{r} = \vec{\gamma}^{-1}\left(\mathbf{n} + \frac{\alpha}{2}\mathbf{d}\right), \mathbf{n} \in \mathbb{Z}^3\right\}, \tag{A2}$$

where

$$\alpha = 1 + \frac{m_K^2 - m_\pi^2}{E_{\mathrm{CM}}^2}.$$

The operation $\hat{\gamma}^{-1}$ is defined in Eq. (8). The zeta function $\mathcal{Z}^{\mathbf{d}}_{20}(1; q^2)$ is used to evaluate the p-wave scattering phase shift in the present work.

First we consider $q^2 > 0$, and we separate the summation in $\mathcal{Z}_{20}$ into two parts as

$$\sum_{\mathbf{r}\in P_{\mathbf{d}}} \frac{\mathcal{Y}_{20}(\mathbf{r})}{(r^2 - q^2)^s} = \sum_{r^2<q^2} \frac{\mathcal{Y}_{20}(\mathbf{r})}{(r^2 - q^2)^s} + \sum_{r^2>q^2} \frac{\mathcal{Y}_{20}(\mathbf{r})}{(r^2 - q^2)^s}, \tag{A3}$$

where the summation over $\mathbf{r}$ is performed with $\mathbf{r} \in P_{\mathbf{d}}$ denoted in Eq. (A2). The second term can be expressed in an integral form:

$$\begin{aligned}
\sum_{r^2>q^2} \frac{\mathcal{Y}_{20}(\mathbf{r})}{(r^2 - q^2)^s} &= \frac{1}{\Gamma(s)} \sum_{r^2>q^2} \mathcal{Y}_{20}(\mathbf{r}) \left[\int_0^1 \mathrm{d}t t^{s-1} e^{-t(r^2-q^2)} \right. \\
&\quad \left. + \int_1^\infty \mathrm{d}t t^{s-1} e^{-t(r^2-q^2)}\right] \\
&= \frac{1}{\Gamma(s)} \int_0^1 \mathrm{d}t t^{s-1} e^{q^2 t} \sum_{\mathbf{r}\in P_{\mathbf{d}}} \mathcal{Y}_{20}(\mathbf{r}) e^{-r^2 t} \\
&\quad - \sum_{r^2<q^2} \frac{\mathcal{Y}_{20}(\mathbf{r})}{(r^2 - q^2)^s} + \sum_{\mathbf{r}\in P_{\mathbf{d}}} \mathcal{Y}_{20}(\mathbf{r}) \frac{e^{-(r^2-q^2)}}{(r^2 - q^2)^s}.
\end{aligned} \tag{A4}$$

The second term nicely counteracts the first term in Eq. (A3). Using the Poisson resummation formula, the first term leads to

$$\text{first term} = \frac{1}{\Gamma(s)} \int_0^1 dt t^{s-1} e^{tq^2} \sum_{\mathbf{n}\in\mathbb{Z}^3} f_{\mathbf{n}},$$
$$f_{\mathbf{n}} \equiv \int d^3\mathbf{x}\, \mathcal{Y}_{20}(\mathbf{r}) e^{-t|\mathbf{r}|^2 + i2\pi\mathbf{n}\cdot\mathbf{x}}, \tag{A5}$$

where $\mathbf{r} = \hat{\gamma}^{-1}(\mathbf{x} + \frac{1}{2}\alpha\mathbf{d})$. We transform the integration variable from $\mathbf{x}$ to $\mathbf{r}$ by considering $d^3\mathbf{x} = \gamma d^3\mathbf{r}$ and $\mathbf{x} = \hat{\gamma}\mathbf{r} - \frac{1}{2}\alpha\mathbf{d}$. Then we can separate terms that depend only on $\mathbf{r}$:

$$f_{\mathbf{n}} \equiv \gamma e^{-i\pi\alpha\mathbf{n}\cdot\mathbf{d}} \int d^3\mathbf{r}\, \mathcal{Y}_{20}(\mathbf{r}) e^{-t|\mathbf{r}|^2 + i2\pi\hat{\gamma}\mathbf{n}\cdot\mathbf{r}}.$$

Letting $\mathbf{k} \equiv \pi\hat{\gamma}\mathbf{n}$, we rewrite the above equation as

$$f_{\mathbf{n}} \equiv \gamma e^{-i\pi\alpha\mathbf{n}\cdot\mathbf{d}} e^{-k^2/t^2} \int d^3\mathbf{r}\, \mathcal{Y}_{20}(\mathbf{r}) e^{-t(\mathbf{r} - i\mathbf{k}/t)^2},$$

where $\mathbf{r} = (x, y, z)$. By performing a variable substitution, namely, $\mathbf{r} - i\mathbf{k}/t \to \mathbf{r}$, we can strictly verify that

$$\begin{aligned}
\int d^3\mathbf{r} x^2 e^{-t(\mathbf{r} - i\mathbf{k}/t)^2} &= \frac{2\pi}{t} \int_0^\infty dx \left(x^2 - \frac{k_x^2}{t^2}\right) e^{-tx^2} \\
&= \left(\frac{\pi}{t}\right)^{3/2} \left(\frac{1}{2t} - \frac{k_x^2}{t^2}\right), \\
\int d^3\mathbf{r} y^2 e^{-t(\mathbf{r} - i\mathbf{k}/t)^2} &= \left(\frac{\pi}{t}\right)^{3/2} \left(\frac{1}{2t} - \frac{k_y^2}{t^2}\right), \\
\int d^3\mathbf{r} z^2 e^{-t(\mathbf{r} - i\mathbf{k}/t)^2} &= \left(\frac{\pi}{t}\right)^{3/2} \left(\frac{1}{2t} - \frac{k_z^2}{t^2}\right).
\end{aligned} \tag{A6}$$

We finally obtain

$$f_{\mathbf{n}} \equiv -\gamma e^{-i\pi\alpha\mathbf{n}\cdot\mathbf{d}} e^{-k^2/t^2} \frac{\pi^{3/2}}{t^{7/2}} \mathcal{Y}_{20}(\mathbf{k}),$$

where $\mathcal{Y}_{20}(\mathbf{k}) \equiv k^2 Y_{20}(\Omega_k)$. Now we can rewrite the first term in Eq. (A4) as

$$\text{first term} = \frac{\gamma}{\Gamma(s)} \int_0^1 \mathrm{d}t t^{s-1} e^{tq^2} \frac{\pi^{\frac{3}{2}}}{t^{\frac{7}{2}}} \sum_{\mathbf{n}\in\mathbb{Z}^3} (\pi\hat{\gamma}\mathbf{n})^2 \times Y_{20}(\Omega_k) e^{i\pi\alpha\mathbf{n}\cdot\mathbf{d}} e^{-(i\pi\hat{\gamma}\mathbf{n})^2/t}. \tag{A7}$$

After collecting all terms we arrive at the representation of the zeta function at $s = 1$,

$$\begin{aligned}
\mathcal{Z}_{20}^{\mathbf{d}}(1; q^2) = &\sum_{\mathbf{r}\in P_{\mathbf{d}}} r^2 Y_{20}(\Omega_r) \frac{e^{-(r^2 - q^2)}}{r^2 - q^2} \\
&- \int_0^1 \mathrm{d}t e^{tq^2} \frac{\pi^{\frac{3}{2}}}{t^{\frac{7}{2}}} \sum_{\mathbf{n}\in\mathbb{Z}^3} (\pi\hat{\gamma}\mathbf{n})^2 \\
&\times Y_{20}(\Omega_k) e^{-i\pi\alpha\mathbf{n}\cdot\mathbf{d}} e^{-(\pi\hat{\gamma}\mathbf{n})^2/t}.
\end{aligned} \tag{A8}$$

For the case of $q^2 \leq 0$, it is not necessary for us to segregate the summation in $\mathcal{Z}_{20}^{\mathbf{d}}(s; q^2)$, and it can also be expressed in an integral form. Performing the same procedures, we obtain the same expression as in Eq. (A8). Hence, Eq. (A8) is applicable for both cases.

Substituting $\mathbf{d} = (0, 0, 1)$ into Eq. (A8), we arrive at the representation of the zeta function $\mathcal{Z}_{20}^{\mathbf{d}}(s; q^2)$ appearing in Eq. (12):

$$\begin{aligned}
\mathcal{Z}_{20}^{\mathbf{d}}(1; q^2) = &\sum_{\mathbf{r}\in P_{\mathbf{d}}} r^2 Y_{20}(\Omega_r) \frac{e^{-(r^2 - q^2)}}{r^2 - q^2} \\
&- \int_0^1 \mathrm{d}t e^{tq^2} \frac{\pi^{\frac{3}{2}}}{t^{\frac{7}{2}}} \sum_{\mathbf{n}\in\mathbb{Z}^3} (\pi\hat{\gamma}\mathbf{n})^2 Y_{20}(\Omega_k) \\
&\times \cos(\pi\alpha\mathbf{n}\cdot\mathbf{d}) e^{-(\pi\hat{\gamma}\mathbf{n})^2/t},
\end{aligned} \tag{A9}$$

where the imaginary part of the zeta function is neatly canceled out.

We also note that the general numerical evaluation of the zeta function $\mathcal{Z}_{lm}^{\mathbf{d}}(s; q^2)$ has been derived in Refs. [21,22]. We numerically compared both these representations of the zeta $\mathcal{Z}_{20}(1; q^2)$ function with this representation, and found reasonable agreement.

[1] J. Beringer *et al.* (Particle Data Group Collaboration), Phys. Rev. D **86**, 010001 (2012).
[2] M. Ablikim *et al.* (BES Collaboration), Phys. Lett. B **633**, 681 (2006).
[3] J. Z. Bai *et al.* (BES Collaboration), arXiv:hep-ex/0304001.
[4] D. R. Boito, R. Escribano, and M. Jamin, J. High Energy Phys. 09 (2010) 031.
[5] R. E. Mitchell *et al.* (CLEO Collaboration), Phys. Rev. D **79**, 072008 (2009).
[6] B. Aubert *et al.* (*BABAR* Collaboration), Phys. Rev. D **76**, 012008 (2007).
[7] S. A. Gottlieb, P. B. MacKenzie, H. B. Thacker, and D. Weingarten, Nucl. Phys. **B263**, 704 (1986).
[8] S. A. Gottlieb, P. B. Mackenzie, H. B. Thacker, and D. Weingarten, Phys. Lett. **134B**, 346 (1984).
[9] N. Vasanti, Nucl. Phys. **B118**, 533 (1977).
[10] R. D. Loft and T. A. DeGrand, Phys. Rev. D **39**, 2692 (1989).
[11] X. Feng, K. Jansen, and D. B. Renner, Phys. Rev. D **83**, 094505 (2011).
[12] R. L. Altmeyer, M. Gockeler, R. Horsley, E. Laermann, G. Schierholz, and P. M. Zerwas, Z. Phys. C **68**, 443 (1995).

[13] C. McNeile *et al.* (UKQCD Collaboration), Phys. Lett. B **556**, 177 (2003).
[14] S. Aoki *et al.* (*CP*-PACS Collaboration), Phys. Rev. D **76**, 094506 (2007).
[15] N. Ishizuka (PACS-CS Collaboration), Proc. Sci. LATTICE (2011) 125.
[16] S. Aoki *et al.* (CS Collaboration), Phys. Rev. D **84**, 094505 (2011).
[17] C. B. Lang, D. Mohler, S. Prelovsek, and M. Vidmar, Phys. Rev. D **84**, 054503 (2011).
[18] J. Frison *et al.*, Proc. Sci. LATTICE (2010) 139.
[19] K. Rummukainen and S. A. Gottlieb, Nucl. Phys. **B450**, 397 (1995).
[20] Z. Davoudi and M. J. Savage, Phys. Rev. D **84**, 114502 (2011).
[21] Z. Fu, Phys. Rev. D **85**, 014506 (2012).
[22] L. Leskovec and S. Prelovsek, Phys. Rev. D **85**, 114507 (2012).
[23] M. Gockeler, R. Horsley, M. Lage, U.-G. Meissner, P. E. L. Rakow, A. Rusetsky, G. Schierholz, and J. M. Zanotti, arXiv:1206.4141.
[24] M. Doring, U. G. Meissner, E. Oset, and A. Rusetsky, Eur. Phys. J. A **48**, 114 (2012).
[25] M. T. Hansen and S. R. Sharpe, Phys. Rev. D **86**, 016007 (2012).
[26] V. Bernard, D. Hoja, U. G. Meissner, and A. Rusetsky, J. High Energy Phys. 09 (2012) 023.
[27] J. Nebreda and J. R. Peláez, Phys. Rev. D **81**, 054035 (2010).
[28] Z. Fu and K. Fu (to be published).
[29] Z. Fu, J. High Energy Phys. 07 (2012) 142.
[30] Z. Fu, J. High Energy Phys. 01 (2012) 017.
[31] Z. Fu, Phys. Rev. D **85**, 074501 (2012).
[32] C. Bernard *et al.*, Phys. Rev. D **83**, 034503 (2011).
[33] A. Bazavov *et al.*, Rev. Mod. Phys. **82**, 1349 (2010).
[34] M. Lüscher, Nucl. Phys. **B354**, 531 (1991).
[35] L. Lellouch and M. Luscher, Commun. Math. Phys. **219**, 31 (2001).
[36] M. Luscher and U. Wolff, Nucl. Phys. **B339**, 222 (1990).
[37] T. Yamazaki *et al.* (*CP*-PACS Collaboration), Phys. Rev. D **70**, 074513 (2004).
[38] M. Doring, U.-G. Meissner, E. Oset, and A. Rusetsky, Eur. Phys. J. A **47**, 139 (2011).
[39] S. R. Sharpe, R. Gupta, and G. W. Kilcup, Nucl. Phys. **B383**, 309 (1992).
[40] Y. Kuramashi, M. Fukugita, H. Mino, M. Okawa, and A. Ukawa, Phys. Rev. Lett. **71**, 2387 (1993).
[41] M. Fukugita, Y. Kuramashi, M. Okawa, H. Mino, and A. Ukawa, Phys. Rev. D **52**, 3003 (1995).
[42] M. Fukugita, Y. Kuramashi, H. Mino, M. Okawa, and A. Ukawa, Phys. Rev. Lett. **73**, 2176 (1994).
[43] J. Nagata, S. Muroya, and A. Nakamura, Phys. Rev. C **80**, 045203 (2009).
[44] C. Miao, X. Du, G. Meng, and C. Liu, Phys. Lett. B **595**, 400 (2004).
[45] S. R. Beane, P. F. Bedaque, T. C. Luu, K. Orginos, E. Pallante, A. Parreno, and M. J. Savage, Phys. Rev. D **74**, 114503 (2006).
[46] K. Sasaki *et al.* (PACS-CS Collaboration), Prog. Theor. Phys. Suppl. **186**, 187 (2010).
[47] C. B. Lang, L. Leskovec, D. Mohler, and S. Prelovsek, Phys. Rev. D **86**, 054508 (2012).
[48] Z. Fu, Eur. Phys. J. C **72**, 2159 (2012).
[49] Z. Fu, Commun. Theor. Phys. **57**, 78 (2012).
[50] T. DeGrand and C. DeTar, *Lattice Methods for Quantum Chromodynamics* (World Scientific, Singapore, 2006).
[51] S. Dürr, C. Hoelbling, and U. Wenger, Phys. Rev. D **70**, 094502 (2004).
[52] C. Bernard, Phys. Rev. D **73**, 114503 (2006).
[53] C. Bernard, M. Golterman, Y. Shamir, and S. R. Sharpe, Phys. Lett. B **649**, 235 (2007).
[54] M. Creutz, Phys. Lett. B **649**, 241 (2007).
[55] C. Bernard, M. Golterman, and Y. Shamir, Phys. Rev. D **73**, 114511 (2006).
[56] M. Creutz, Phys. Lett. B **649**, 230 (2007).
[57] S. Dürr and C. Hoelbling, Phys. Rev. D **71**, 054501 (2005).
[58] S. Dürr and C. Hoelbling, Phys. Rev. D **74**, 014513 (2006).
[59] A. Hasenfratz and R. Hoffmann, Phys. Rev. D **74**, 014511 (2006).
[60] C. W. Bernard, T. Burch, K. Orginos, D. Toussaint, T. DeGrand, C. DeTar, S. Datta, S. Gottlieb, U. Heller, and R. Sugar, Phys. Rev. D **64**, 054506 (2001).
[61] C. Aubin, C. Bernard, C. DeTar, J. Osborn, S. Gottlieb, E. Gregory, D. Toussaint, U. Heller, J. Hetrick, and R. Sugar, Phys. Rev. D **70**, 094505 (2004).
[62] C. DeTar (private communication).
[63] C. W. Bernard, T. Draper, G. Hockney, and A. Soni, in *Proceedings of a NATO Workshop on Lattice Gauge Theories-a Challenge in Large Scale Computing, Wuppertal, 1985* (Plenum Press, New York, 1985), p. 199.
[64] C. W. Bernard, T. Draper, G. Hockney, A. M. Rushton, and A. Soni, Phys. Rev. Lett. **55**, 2770 (1985).
[65] I. T. Drummond, S. Duane, and R. R. Horgan, Nucl. Phys. **B220**, 119 (1983).
[66] S.-J. Dong and K.-F. Liu, Phys. Lett. B **328**, 130 (1994).
[67] M. Foster and C. Michael, Phys. Rev. D **59**, 074503 (1999).
[68] D. Barkai, K. J. M. Moriarty, and C. Rebbi, Phys. Lett. **156B**, 385 (1985).
[69] A. Mihaly, H. R. Fiebig, H. Markum, and K. Rabitsch, Phys. Rev. D **55**, 3077 (1997).
[70] A. Mihály, Ph.D. thesis, Lajos Kossuth University, Debrecen, 1998.
[71] R. Gupta, A. Patel, and S. R. Sharpe, Phys. Rev. D **48**, 388 (1993).
[72] X. Feng, K. Jansen, and D. B. Renner, Phys. Lett. B **684**, 268 (2010).
[73] T. Umeda, Phys. Rev. D **75**, 094502 (2007).
[74] M. G. Alford, W. Dimm, G. P. Lepage, G. Hockney, and P. B. Mackenzie, Phys. Lett. B **361**, 87 (1995).
[75] D. B. Kaplan, Phys. Lett. B **288**, 342 (1992); Y. Shamir, Nucl. Phys. **B406**, 90 (1993); Phys. Rev. D **59**, 054506 (1999).
[76] V. Bernard, N. Kaiser, and U. G. Meissner, Nucl. Phys. **B357**, 129 (1991).
[77] G. P. Lepage, in *Proceedings of TASI '89 Summer School*, edited by T. DeGrand and D. Toussaint (World Scientific, Singapore, 1990), p. 97.
[78] H.-X. Chen and E. Oset, arXiv:1202.2787.